Supplementary Information

S1 Remapping of observational data into JSBACH plant functional types

Vegetation productivity in JSBACH has been shown to be higher compared to observations (Anav et al., 2013; Todd-Brown et al., 2013). We compared the productivity of JSBACH within coupled model in the historical simulation of the fifth phase of the Coupled Model Intercomparison Project (CMIP5), and an additional offline simulation with JSBACH driven by CRU climate with observation-based plant productivity. The productivity in these two simulations is higher compared to that in the observational-data (see section S2).

For the obs_drvn simulations, we used global maps of leaf area index (LAI) that are derived from the MODIS satellite and the gross primary production (GPP) derived by extending flux net tower measurements using machine learning algorithms for the year 2001 to 2010 (Tramontana et al., 2016). Vegetation classification for the GPP and LAI data is based on the International Geosphere Biosphere Programme (IGBP) classification, while our DGVM uses plant functional types (PFTs) to represent global vegetation distribution. Using classification rules by Pongratz et al. (2008) and Poulter et al. (2011), we remapped the cover fraction map used in deriving the GPP and LAI into JSBACH PFTs (see cover fraction map description in Friedl et al., 2010, Table. 1). Table S1 shows the classification rules used in remapping the cover fraction map and the PFTs they are allocated to. Since the remapping classification rules do not include remapping to pasture, the cover fraction maps for the pastures were taken from JSBACHs' cover fraction maps as used for the global annual carbon budget simulations (Le Quéré et al., 2015). The fractions for the pastures were then obtained by reducing the remapped grasses cover fractions. For the idealized simulations, we scale the remapped cover fractions proportionally to create idealized cover fraction maps for forest, crop, grass and pasture. The relative distributions of the different PFTs belonging to one vegetation type are kept at the relative distribution obtained from the remapped cover fraction map.

We use the newly reconstructed cover fraction map for remapping the GPP and LAI. For every grid cell where there is a cover fraction value for a given PFT, it is required that there is a LAI and GPP value. Each PFT in JSBACH had an observation vegetation type it can be linked to directly. For example, the tropical evergreen forests correspond to the evergreen broadleaf forests in the observations classification (Table S1). For these grid cells, the GPP and LAI of the PFT is taken directly from the observation classification. We assume that grasses and pastures have equal productivity within a given grid cell. Hence the GPP for grasses and pastures is taken from grasslands GPP in these grid cells. If the LAI and GPP value for the remapped PFT is missing in the grid cell and the PFT has a cover fraction, the GPP and LAI value for the closest neighbouring grid cell is assigned. An assumption is made that the productivity of, for example, a tropical deciduous forest in an area covered with forests alone is the same as that of a forest in a savanna.

Unlike for GPP, globally there are no observations on autotrophic respiration, which makes it difficult to obtain NPP from GPP. We derive annual GPP to NPP ratios for each PFT from a simulation where JSBACH was driven by CRU climate. In this case, we assume that the model biases in GPP and autotrophic respiration, both being dependent on productivity, largely cancel. These ratios are used to scale the remapped GPP to NPP.

We test how our nearest neighbour approach influences the relative and absolute changes in soil carbon discussed in our results section. We select only the grid cells where the GPP and LAI is not obtained from the nearest neighbouring grid cells and compare the results to those obtained by considering the entire regions. Figure S5 shows that the relative changes simulated by selecting only these grid cells do not differ much from the changes simulated by considering the entire regions.

S2 Comparison of global GPP and NPP values

We compared the GPP remapped from observations with the original GPP and the GPP from the historical simulations in CMIP5 (Giorgetta et al., 2013) and simulations with JSBACH driven by CRU climate. Table S2 shows that the JSBACH GPP is quite large compared to the observation-based GPP. In addition, we compared the NPP values obtained using the JSBACH derived ratio with the NPP that we would have obtained by assuming 50% autotrophic respiration costs as done in previous studies (Carvalhais et al., 2014). Table S3 shows that the global NPP value obtained using the JSBACH derived ratio differs slightly from the NPP obtained by assuming 50% respiration costs.

Table S1: Rules for the reclassification of the vegetation map to the 12 JSBACH Plant functional types cover fractions. T_{min} represents the mean temperature of the coldest month

Observation Classification	**Classification rule**	**JSBACH PFT**	**Classification source**
Evergreen needleleaf forests		Extratropical evergreen forests	
Evergreen broadleaf forests		Tropical evergreen forests	
Deciduous needleleaf forests		Extratropical deciduous forests	
Deciduous broadleaf forests	$\|latitude\|$ >30°	Extratropical deciduous forests	
	$\|latitude\|$ ≤30°	Tropical deciduous forests	
Mixed forest	$\|latitude\|$ >30°	50% Extratropical evergreen forests 50% Extratropical deciduous forests	Table 6 in Poulter et al. (2011) without the distinction of needleleaf and broadleaf trees
	$\|latitude\|$ ≤30°	50% Tropical evergreen forests 50% Tropical deciduous forests	
Savanna woody[1]	$latitude$ >30°	25% Extratropical evergreen forests 25% Extratropical deciduous forests 50% C3 grasses and C4 grasses[6]	Table 6 in Poulter et al. (2011) without the distinction of needleleaf and broadleaf trees
	$latitude$ ≤30°	25% Tropical evergreen forests 25% Tropical deciduous forests 50% C3 grasses and C4 grasses[6]	
Savannas[2]	$latitude$ >30°	20% Extratropical evergreen forests 20% Extratropical deciduous forests 60% C3 grasses and C4 grasses[6]	Table 6 in Poulter et al. (2011) without the distinction of the needleleaf and the broadleaf trees
	$latitude$ ≤30°	20% Tropical evergreen forests 20% Tropical deciduous forests 60% C3 grasses and C4 grasses[6]	
Grasslands		C3 grasses and C4 grasses[6]	
Closed shrublands[3]	T_{min} <-10°	80% Deciduous shrubs 20% C3 grasses and C4 grasses[6]	Table 5 in Pongratz et al. (2008) with the assumption that summergreen shrubs are the same as deciduous shrubs
	T_{min} ≥-10°	80% Rain shrubs 20% C3 grasses and C4 grasses[6]	
Open shrublands[4]	T_{min} <-10°	40% deciduous shrubs 60% C3 grasses and C4 grasses[6]	Table 5 in Pongratz et al. (2008) with the assumption that summergreen shrubs are same as deciduous shrubs
	T_{min} ≥-10°	40% rain shrubs 60% C3 grasses and C4 grasses[6]	
C3 croplands		Crops	
C4 croplands		Crops	
Croplands with natural mosaic[5]	$latitude$ >30°	34% Extratropical evergreen forests 34% Extratropical deciduous forests	Table 6 in Poulter et al. (2011) with the assumption that manmade grasses are the same as crops

Table S1 – Continued

Observation Classification	Classification rule	JSBACH PFT	Classification source
		16% C3 grasses and C4 grasses[6] 16% Crops	
	$latitude \leq 30^{\circ}$	34% Tropical evergreen forests 34% Tropical deciduous forests 16% C3 grasses and C4 grasses[6] 16% Crops	

[1]Lands with herbaceous and other understorey systems and with forest cover between 30-60% (D'Souza, 2000)

[2]Lands with herbaceous and other understorey systems and with forest cover between 10-30% (D'Souza, 2000)

[3]Lands with woody vegetationn less than 2 metres tall and with shrub canopy cover greater than 60% (D'Souza, 2000)

[4]Lands with woody vegetation less than 2 metres tall and with shrub canopy between 10-60% (D'Souza, 2000)

[5]Lands with a mosaic of croplands, forests, shrublands and grasslands in which no one component comprises more than 60% of the land scape (D'Souza, 2000)

[6]A temperature criterion based on the temperature of the warmest month between 2001-2010 from CRU-NCEP data set is applied to define areas where we can have co-existence of C3 and C4 grasses between ($17\,^{\circ}$C and $29\,^{\circ}$C) and areas where either of them exists

Table S2. Global remapped GPP in Pg C compared with GPP from different JSBACH simulations.

GPP source	Global GPP value
Observations	118.32
Observations remapped into PFTs	110.75
JSBACH CMIP5	179.97
JSBACH driven with CRU climate	185.37

Table S3. Global remapped NPP in Pg C

NPP source	Global NPP value
Observations remapped with JSBACH ratio	54.51
Observations remapped with NPP:GPP ratio of 50%	55.31

Table S4. Contribution of the mean absolute changes over the sampled ages to the equilibrium absolute changes for the jsbach_drvn_harv simulation.

Land-use change	Mean age (years)	Sampled age changes (kgC m^{-2})	Equilibrium changes (kgC m^{-2})	Contribution (%)
Crop to forest (temperate)	40.28	2.39	10.83	22
Crop to grass (temperate)	21.7	0.68	2.98	23
Forest to crop (temperate)	50.21	-3.77	-11.50	38
Grass to crop (temperate)	39.69	-0.50	-2.61	19
Forest to crop (tropics)	22.5	-1.45	-8.67	17
Forest to pasture (tropics)	20.67	-1.74	-5.63	31

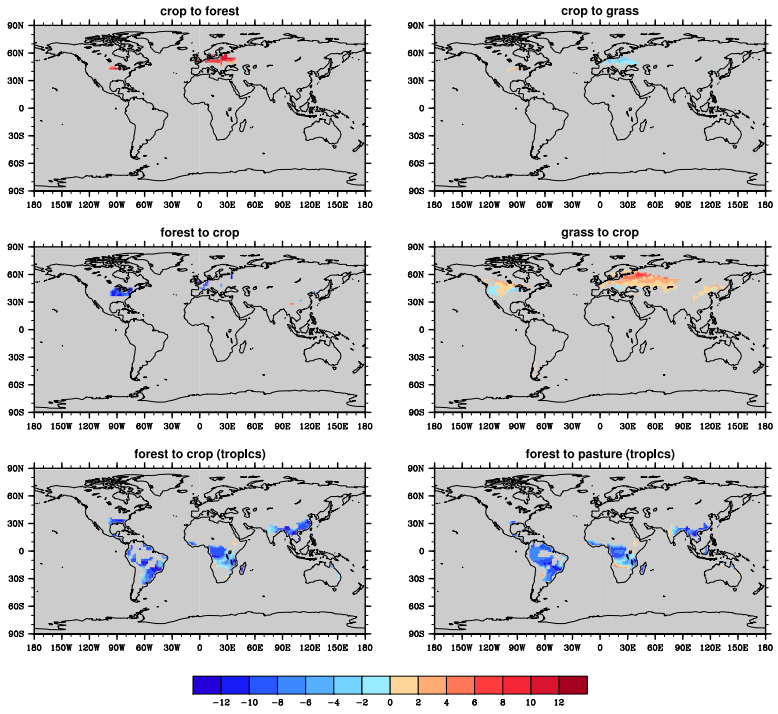

Figure S1. Equilibrium absolute changes in soil carbon in kgC m^{-2} for the different land-use changes in the jsbach_drvn simulation. The regions are based on the climate criterion (precipitation and temperature) of the meta-data.

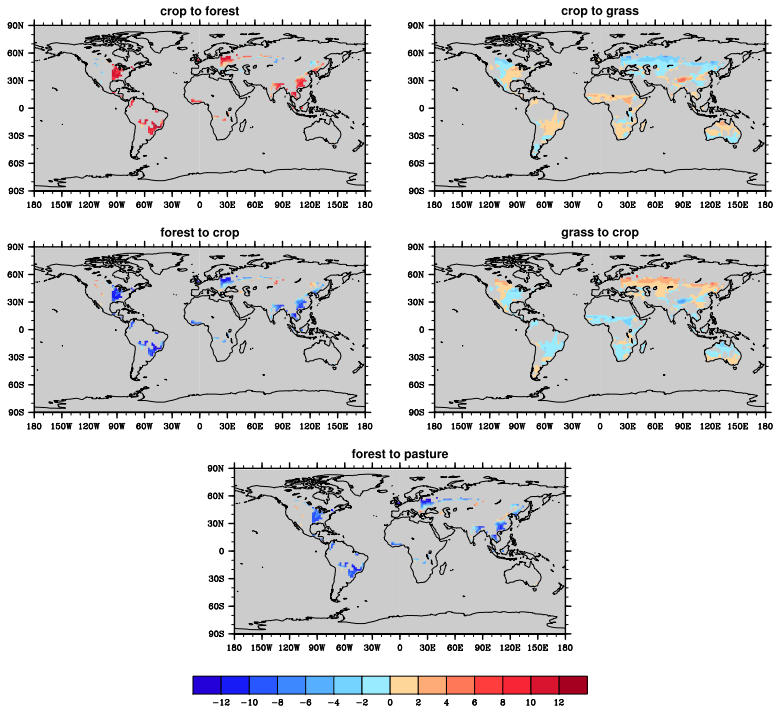

Figure S2. Equilibrium absolute changes in soil carbon in kgC m^{-2} for the different land-use changes in the jsbach_drvn simulation. The regions are based on where land-use change has taken place historically between 1850 and 2005.

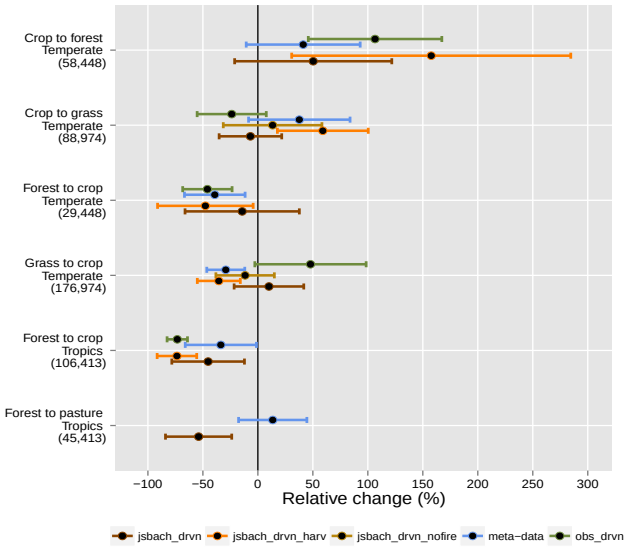

(a) Mean equilibrium relative changes

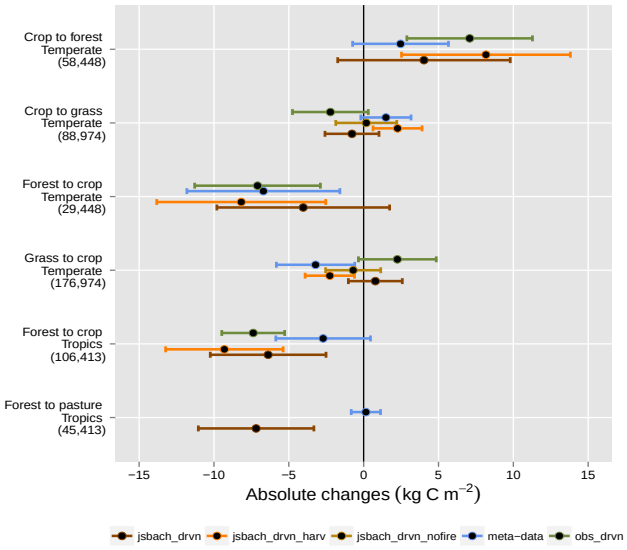

(b) Mean equilibrium absolute changes

Figure S3. Mean simulated equilibrium relative (a) and absolute changes in soil carbon (b) for the regions selected based on where land use change has taken place historically compared to the mean changes in the meta-data (regions in Fig. S2). The first number in the parenthesis represents the number of sites in the meta-data and the second is the number of grid cells fulfilling the climate range in the meta-data. The bars represent the standard deviation.

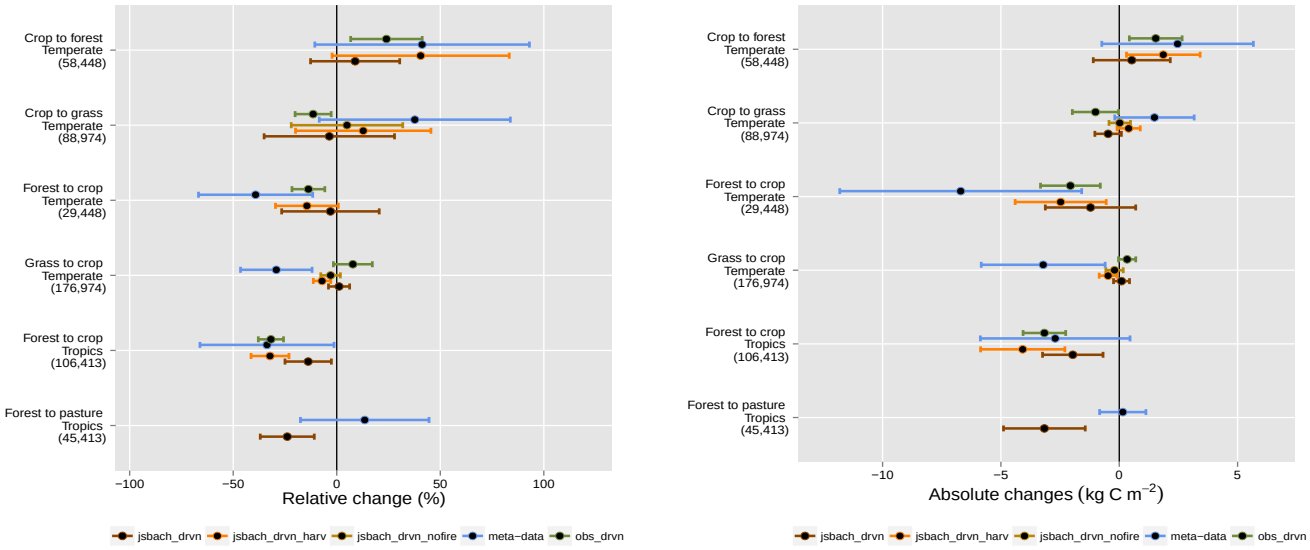

(a) Mean equilibrium relative changes

(b) Mean equilibrium absolute changes

Figure S4. Mean simulated relative (a) and absolute changes in soil carbon (b) over the sampled ages represented by the meta-data compared to the mean changes for the meta-data. The first number in the parenthesis represents the number of studies in the meta-data and the second is the number of grid cells from the global simulation that fulfil the climate-criterion in the meta-data (regions in supplementary material Fig. S1). The dots represent the mean changes and the bars represent the standard deviation.

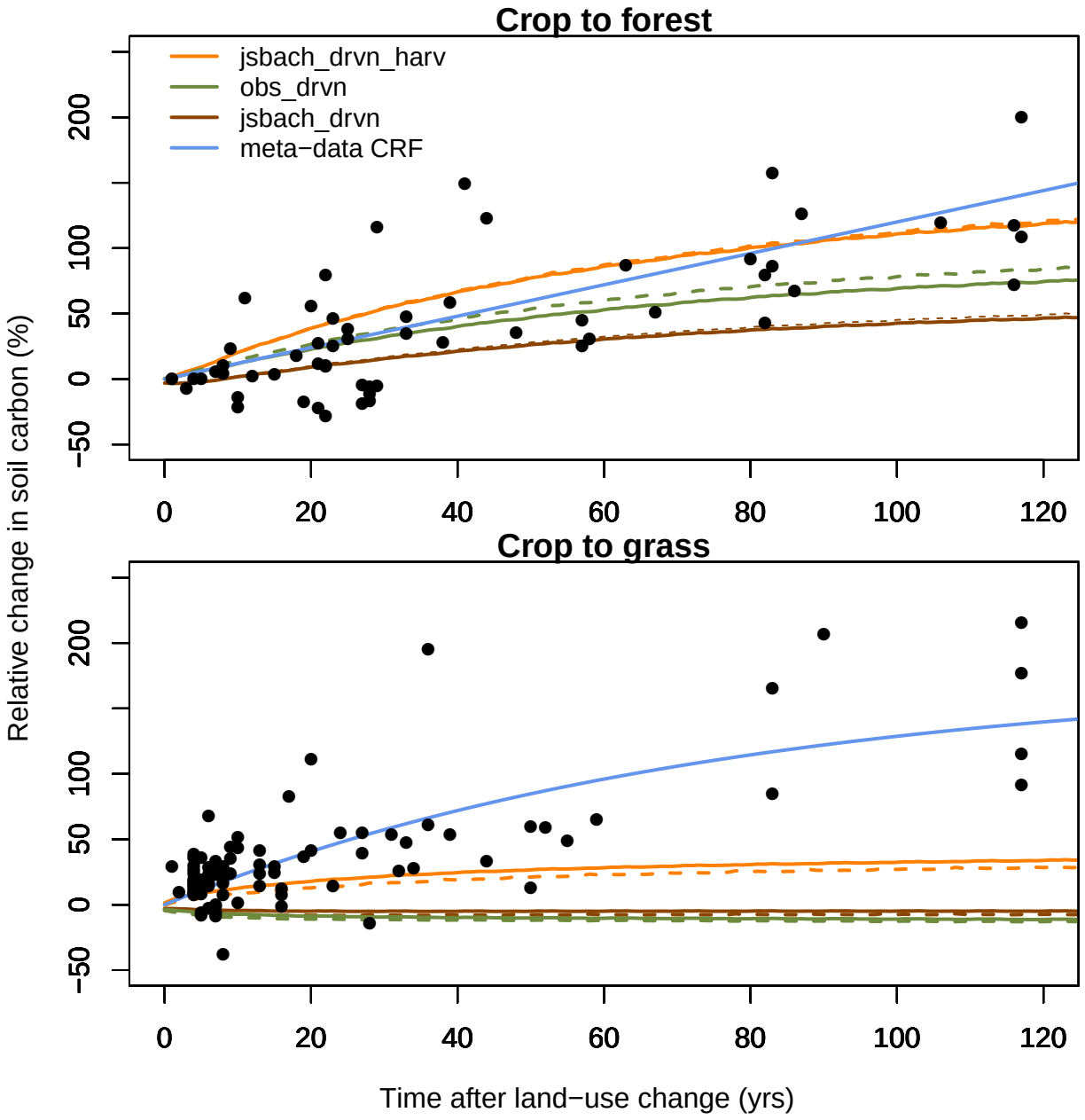

Figure S5. Mean simulated transient relative changes in soil carbon compared to the individual observations (black dots) and generalized carbon response functions (CRF) as in Poeplau et al. (2011) for the crop to grass and crop to forest transition. The dotted lines represent the regions where there was no nearest neighbour search for the GPP and LAI for the observations remapping in the considered climate regions.

References

Anav, A., Friedlingstein, P., Kidston, M., Bopp, L., Ciais, P., Cox, P., Jones, C., Jung, M., Myneni, R., and Zhu, Z.: Evaluating the Land and Ocean Components of the Global Carbon Cycle in the CMIP5 Earth System Models, Journal of Climate, 26, 6801–6843, doi:10.1175/JCLI-D-12-00417.1, 2013.

Carvalhais, N., Forkel, M., Khomik, M., Bellarby, J., Jung, M., Migliavacca, M., Mu, M., Saatchi, S., Santoro, M., Thurner, M., Weber, U., Ahrens, B., Beer, C., Cescatti, A., Randerson, J. T., and Reichstein, M.: Global covariation of carbon turnover times with climate in terrestrial ecosystems., Nature, 514, 213–7, doi:10.1038/nature13731, 2014.

D'Souza, G.: FRA 2000: Forest cover mapping & monitoring with NOAA-AVHRR & other Coarse Spatial resolution sensors, 2000.

Friedl, M. A., Sulla-Menashe, D., Tan, B., Schneider, A., Ramankutty, N., Sibley, A., and Huang, X.: MODIS Collection 5 global land cover: Algorithm refinements and characterization of new datasets, Remote Sensing of Environment, 114, 168–182, doi:10.1016/j.rse.2009.08.016, 2010.

Giorgetta, M. A., Jungclaus, J., Reick, C. H., Legutke, S., Bader, J., Böttinger, M., Brovkin, V., Crueger, T., Esch, M., Fieg, K., Glushak, K., Gayler, V., Haak, H., Hollweg, H.-D., Ilyina, T., Kinne, S., Kornblueh, L., Matei, D., Mauritsen, T., Mikolajewicz, U., Mueller, W., Notz, D., Pithan, F., Raddatz, T., Rast, S., Redler, R., Roeckner, E., Schmidt, H., Schnur, R., Segschneider, J., Six, K. D., Stockhause, M., Timmreck, C., Wegner, J., Widmann, H., Wieners, K.-H., Claussen, M., Marotzke, J., and Stevens, B.: Climate and carbon cycle changes from 1850 to 2100 in MPI-ESM simulations for the Coupled Model Intercomparison Project phase 5, Journal of Advances in Modeling Earth Systems, 5, 572–597, doi:10.1002/jame.20038, 2013.

Le Quéré, C., Moriarty, R., Andrew, R. M., Canadell, J. G., Sitch, S., Korsbakken, J. I., Friedlingstein, P., Peters, G. P., Andres, R. J., Boden, T. A., Houghton, R. A., House, J. I., Keeling, R. F., Tans, P., Arneth, A., Bakker, D. C. E., Barbero, L., Bopp, L., Chang, J., Chevallier, F., Chini, L. P., Ciais, P., Fader, M., Feely, R. A., Gkritzalis, T., Harris, I., Hauck, J., Ilyina, T., Jain, A. K., Kato, E., Kitidis, V., Klein Goldewijk, K., Koven, C., Landschützer, P., Lauvset, S. K., Lefèvre, N., Lenton, A., Lima, I. D., Metzl, N., Millero, F., Munro, D. R., Murata, A., Nabel, J. E. M. S., Nakaoka, S., Nojiri, Y., O'Brien, K., Olsen, A., Ono, T., Pérez, F. F., Pfeil, B., Pierrot, D., Poulter, B., Rehder, G., Rödenbeck, C., Saito, S., Schuster, U., Schwinger, J., Séférian, R., Steinhoff, T., Stocker, B. D., Sutton, A. J., Takahashi, T., Tilbrook, B., van der Laan-Luijkx, I. T., van der Werf, G. R., van Heuven, S., Vandemark, D., Viovy, N., Wiltshire, A., Zaehle, S., and Zeng, N.: Global Carbon Budget 2015, Earth System Science Data, 7, 349–396, doi:10.5194/essd-7-349-2015, 2015.

Poeplau, C., Don, A., Vesterdal, L., Leifeld, J., Van Wesemael, B., Schumacher, J., and Gensior, A.: Temporal dynamics of soil organic carbon after land-use change in the temperate zone - carbon response functions as a model approach, Global Change Biology, 17, 2415–2427, doi:10.1111/j.1365-2486.2011.02408.x, 2011.

Pongratz, J., Reick, C., Raddatz, T., and Claussen, M.: A global land cover reconstruction AD 800 to 1992: Technical description, Tech. rep., Max Planck Insitute for Metereology, Hamburg, Germany, doi:ISSN 1614-1199, 2008.

Poulter, B., Ciais, P., Hodson, E., Lischke, H., Maignan, F., Plummer, S., and Zimmermann, N. E.: Plant functional type mapping for earth system models, Geoscientific Model Development, 4, 993–1010, doi:10.5194/gmd-4-993-2011, 2011.

Todd-Brown, K. E. O., Randerson, J. T., Post, W. M., Hoffman, F. M., Tarnocai, C., Schuur, E. A. G., and Allison, S. D.: Causes of variation in soil carbon simulations from CMIP5 Earth system models and comparison with observations, Biogeosciences, 10, 1717–1736, doi:10.5194/bg-10-1717-2013, 2013.

Tramontana, G., Jung, M., Camps-Valls, G., Ichii, K., Raduly, B., Reichstein, M., Schwalm, C. R., Arain, M. A., Cescatti, A., Kiely, G., Merbold, L., Serrano-Ortiz, P., Sickert, S., Wolf, S., and Papale, D.: Predicting carbon dioxide and energy fluxes across global FLUXNET sites with regression algorithms, Biogeosciences Discussions, pp. 1–33, doi:10.5194/bg-2015-661, 2016.